Original Article

MOLECULAR METABOLISM

Abundance of a metabolically active subpopulation in dedifferentiated adipocytes inversely correlates with body mass index

Jonathan Trujillo-Viera[1,7], Mona C. Wittmann[1,7], Daniel Lam[2], Yang Shen[2], Adhideb Ghosh[3], Falko Noé[3], Anne Hoffmann[4], Coralie Viollet[2], Alec Dick[2], Matthias Blüher[4,5], Jiawei Zhong[6], Lucas Massier[4,6], Christian Wolfrum[3], Holger Klein[2], Heike Neubauer[1], Bradford Hamilton[1,*]

ABSTRACT

Objective: The cellular composition and functionality of adipose tissue are key determinants of metabolic diseases associated with adipose tissue dysregulation, such as obesity. We hypothesized that distinct subpopulations with unique gene expression profiles and functional characteristics exist within human adipocytes.

Methods: Dedifferentiated adipocytes (DFAT), obtained by ceiling culture of human adipocytes, were analyzed using single-cell RNA sequencing (10x Genomics). Clustering analysis identified one subpopulation with a particular gene signature containing muscle cell genes which was further characterized by bulk-sequencing and analyzed alongside different cohorts of human adipose tissue.

Results: This subpopulation, named cluster 7 (C7), was isolated by FACS using two specific surface markers: cluster of differentiation 36 (CD36) and melanoma cell adhesion molecule (MCAM/CD146). Upon differentiation into adipocytes, the FACS-isolated CD36+/CD146+ cells (C7*) showed an increased oxygen consumption rate compared to CD36-/CD146-cells (control cells) and non-sorted cells. Bulk RNA-sequencing revealed important pathways regulated in the differentiated C7* subpopulation that may contribute to its increased metabolic activity. Furthermore, the relative abundance of this specific cluster varied across eleven different human donors, demonstrating an inverse correlation between the proportion of C7* cells and the body mass index (BMI) of the respective donor. Importantly, a subset of genes regulated within this subpopulation also correlates with clinically relevant metabolic parameters, including weight, BMI, glycated hemoglobin, and plasma insulin, when analyzed alongside the gene expression of a large cohort of human subcutaneous adipose tissue (1759 donors).

Conclusion: Our results not only characterize DFAT cells derived from human adipose tissue, but also identify a specific subpopulation with increased energy expenditure that may play a role in body weight control. Future efforts to identify possible therapeutic targets or to promote the enrichment or activation of these energy-burning cells in adipose tissue might be useful in the field of cardiometabolic diseases.

Keywords Energy expenditure; DFAT; Adipocytes; Obesity; CD36; CD146

1. INTRODUCTION

A holistic understanding of adipose tissue at the cellular level can provide important insights and tools for developing therapies to treat metabolic diseases including obesity, diabetes, and metabolic dysfunction-associated steatohepatitis. The advancement and refinement of next-generation sequencing techniques have enabled unraveling the heterogeneity of specific tissues [1]. Recent studies have established informative atlases of human and mouse adipose tissue, demonstrating its diversity and complexity across different species, dietary conditions, and in obesity [2,3]. Single-cell and single-nucleus analyses have enhanced our understanding of adipogenic and thermogenic potential, as well as adipocyte differentiation trajectories. They have also revealed the heterogeneity, not only of adipocytes, but also of precursor and immune cells in adipose tissue [2]. Furthermore, single-cell technologies have led to the identification of specific subpopulations associated with clinical parameters like obesity, BMI, and type 2 diabetes [2,3].

Single-cell/single-nucleus RNA-sequencing (sc/snRNA-seq) of human adipocytes and precursor cells can identify specific subpopulations that might be missed by other approaches but are integral to adipose tissue biology [1,4]. In addition, bulk RNA-sequencing supplements the

[1]Cardio Metabolic Diseases Research, Boehringer Ingelheim Pharma GmbH & Co KG, Biberach an der Riß, Germany [2]Global Computational Biology and Digital Sciences, Boehringer Ingelheim Pharma GmbH and Co. KG, Biberach an der Riß, Germany [3]Institute of Food, Nutrition and Health, ETH Zürich, 8603, Schwerzenbach, Switzerland [4]Helmholtz Institute for Metabolic, Obesity and Vascular Research of the Helmholtz Zentrum München at the University of Leipzig and University Hospital Leipzig, Leipzig, Germany [5]Medical Department III — Endocrinology, Nephrology, Rheumatology, University of Leipzig Medical Center, Leipzig, Germany [6]Department of Medicine Huddinge (H7), Karolinska Institutet, Karolinska University Hospital Huddinge, SE-141 83, Huddinge, Sweden

[7] Equal contribution.

*Corresponding author. E-mail: bradford.hamilton@boehringer-ingelheim.com (B. Hamilton).

Received April 4, 2025 • Accepted April 29, 2025 • Available online 8 May 2025

https://doi.org/10.1016/j.molmet.2025.102161

characterization of such subpopulations *in-vitro* by enabling the study of differentiated adipocytes under conditions that more closely resemble characteristics of naive adipocytes, such as spheroid-cultured adipocytes [5]. Therefore, here we use a combination of both approaches to further explore the biology of dedifferentiated adipocytes (DFAT) and specific subpopulations of interest.

DFAT, which are induced pluripotent stem cells, have been well-studied due to their potential for regenerative medicine, tissue engineering and disease treatment [6]. Numerous advantages, including low immunogenicity, high abundance, accessibility, and cell plasticity, make DFAT an attractive target for developing innovative therapies in different fields [7]. *In-vivo* studies have demonstrated the potential of DFAT for the treatment of diseases associated with heart, kidney, bone, endothelium, and nervous system [6,7]. Nevertheless, these cells are often not well characterized and understood, which is necessary to better understand the cell type and to identify specific subpopulations with therapeutic potential in metabolic diseases. Several efforts have been made to profile specific markers and track transcriptional changes during dedifferentiation and trans-differentiation [6], but there are no reports yet on single-cell resolution. Here, we provide a comprehensive transcriptomic analysis of dedifferentiated adipocytes under different culture conditions and differentiation status. This has the potential to impact the translatability of *in-vitro* studies and the implication of these cells in fields such as tissue transplantation and engineering [5,8]. The identification of one specific subpopulation with increased energy consumption and its correlation with human body weight and other metabolic parameters opens opportunities for further therapeutic developments in obesity, specifically in the field of energy expenditure.

2. RESULTS

2.1. Analysis of stemness, adipogenic, and browning potential of DFAT

DFAT cells are obtained after enzymatic and mechanical dissociation of the extracellular matrix and ceiling culture of the floating adipocytes, which allows them to undergo a reprogramming process that leads them to lose the lipid droplets and to regain their proliferation capacity [9]. We isolated DFAT from subcutaneous adipose tissue of four human donors (with BMI between 20 and 28) and cultured them in maintenance, differentiation, or browning medium. Their adipogenic and browning potential were analyzed by qPCR. We used CD36 as a marker for adipogenesis and triglyceride accumulation [10] as well as UCP1 as a classical browning marker [11] (Supp. Fig 1A-B). In addition, Nile Red staining was used to confirm lipid droplets formation (Supp. Fig 1C). After two weeks in either differentiation or browning media, the increase in *CD36* and *UCP1* respectively demonstrated that despite previously losing lipid droplets and undergoing several passages, these cells still react to adipocyte-inducing stimuli.

We also performed scRNA-seq from DFAT under maintenance medium using four individual donors and integrated the data with a publicly available reference dataset from human white subcutaneous adipose tissue [3]. Unsupervised clustering of human preadipocytes resulted in 12 different clusters (0—11) (Figure 1A). Most of the 12 clusters were reference-based annotated as human adipose stem and progenitor cells (ASPCs), except for cluster 6 which was classified as macrophages and cluster 7 which was annotated as smooth muscle cells (Fig 1B), the latter due to expression of e.g. MYH11, MYLK, ACTA2. Most clusters, with the exception of 6 and 8, were clearly differentiable with 1—2 marker genes (see Suppl. Fig. 2). Clusters 6 and 8 are nevertheless clearly distinct (Fig. 1A), and presumably have a more diffuse transcriptional signature.

Relative abundance of cells in each cluster is shown in Figure 1C. Gene set enrichment analysis for 452 genes upregulated in cluster 7, compared to remaining cells, shows (log_2FC threshold 0.25, P value threshold 0.01) that muscle related processes are enriched (Figure 1D and Supp. Table 1). This demonstrates that the cells in cluster 7 exhibit a set of upregulated genes identified as muscle markers by gene ontology analysis (also shown in Figure 2A). The cells in each cluster were further characterized based on the expression of genes classically known as regulators of differentiation (*PPARG*, *CEBPA* and *CEBPB*) (Fig 1E) and browning/beiging (*PPARGC1A*, *PRDM16*, *TNFRSF9*, *BMP7*, *MYF5*) (Supp. Fig 3) [12,13] or reported as genes associated with commitment, multipotency and adipogenic potential (Fig 1E). Expression of genes associated with adipose precursor cell commitment seems to be variable depending on how this is evaluated. Genes associated with early stages of determination into adipose stem cells, like *DPP4, ALDH1A3, CD55, PDGFRA, PDGFRB,* are expressed in clusters 0 to 5, low expressed in clusters 6 and 8, and unevenly expressed in clusters 7 and 9—11 [3,14—16]. Also, *DPP4* is expressed in a lower percentage of cells compared to the other mentioned genes. Moreover, markers of further commitment into preadipocytes were virtually absent in all clusters (Fig 1E) [3,15—18]. Finally, regarding markers of adipocyte differentiation, *CEBPB* was the only gene expressed in a significant number of cells in most of clusters (except for cluster 6). Other markers of adipocyte differentiation, like PPARG, and CEBPA, were expressed at low levels and/or in a very low percentage of cells (Fig 1E) [4,19]. We also explored our data regarding the current interest in a recently characterized precursor cell type: fibro-inflammatory anti-adipogenic precursors or adipogenesis-regulatory progenitors (Aregs). High expression of a set of genes, including *CLEC11A*, *F3* (*CD142*), *FMO2*, *ABCG1*, and *EPHA3*, has been proposed as marker of Aregs [3,15,20]. However, our data revealed that only *F3* and *CLEC11A* were expressed, while the rest of the genes were absent (Fig 1E). In general, these results indicate that the gene expression profile of DFAT cells (except for clusters 6 and 7) is similar to not fully committed adipocyte precursor cells with multipotency potential. Further experiments might offer deeper understanding in this regard. Also, whilst we found a clear overlap in surface markers between our cells and previously reported DFAT markers, we cannot find markers associated with embryonic stem cells (ESCs) in our data set as it has been reported in the literature (Fig 1F) [6]. Importantly, the gene expression profile of different clusters highlights the similarities and differences of DFAT subpopulations when compared to previous reports in other adipocyte precursor cells [2—4,7]. In addition, cluster 7 is characterized by two surface markers, *CD36* and *MCAM*, that are specifically upregulated in cluster 7 and therefore be used to sort this subpopulation by FACS (Fig 1F).

2.2. Identification and profiling of a subpopulation with an increased metabolic activity

As mentioned before, clusters 6 and 7 showed a gene expression profile that separated them from the reported gene expression signature of adipose precursor cells. Since cluster 6 was annotated as immune cells, we focused our attention on cluster 7 which is characterized by increased expression of genes related to muscle function including *ACTA2*, *ACTG2*, *MYOCD*, *MYLK*, and *MYH11*, among others (Fig 2A). We also identified upregulation of genes involved in fatty acids uptake (*CD36*), fatty acid transport (*FABP4*), fatty acid oxidation (*PRKAA2*, *PRKAB2*, *PRKAG2*), lipolysis (*MGLL*), and a member of the electron transport chain complex I (*NDUFA4L2*) (Fig 2A). Conversely, a

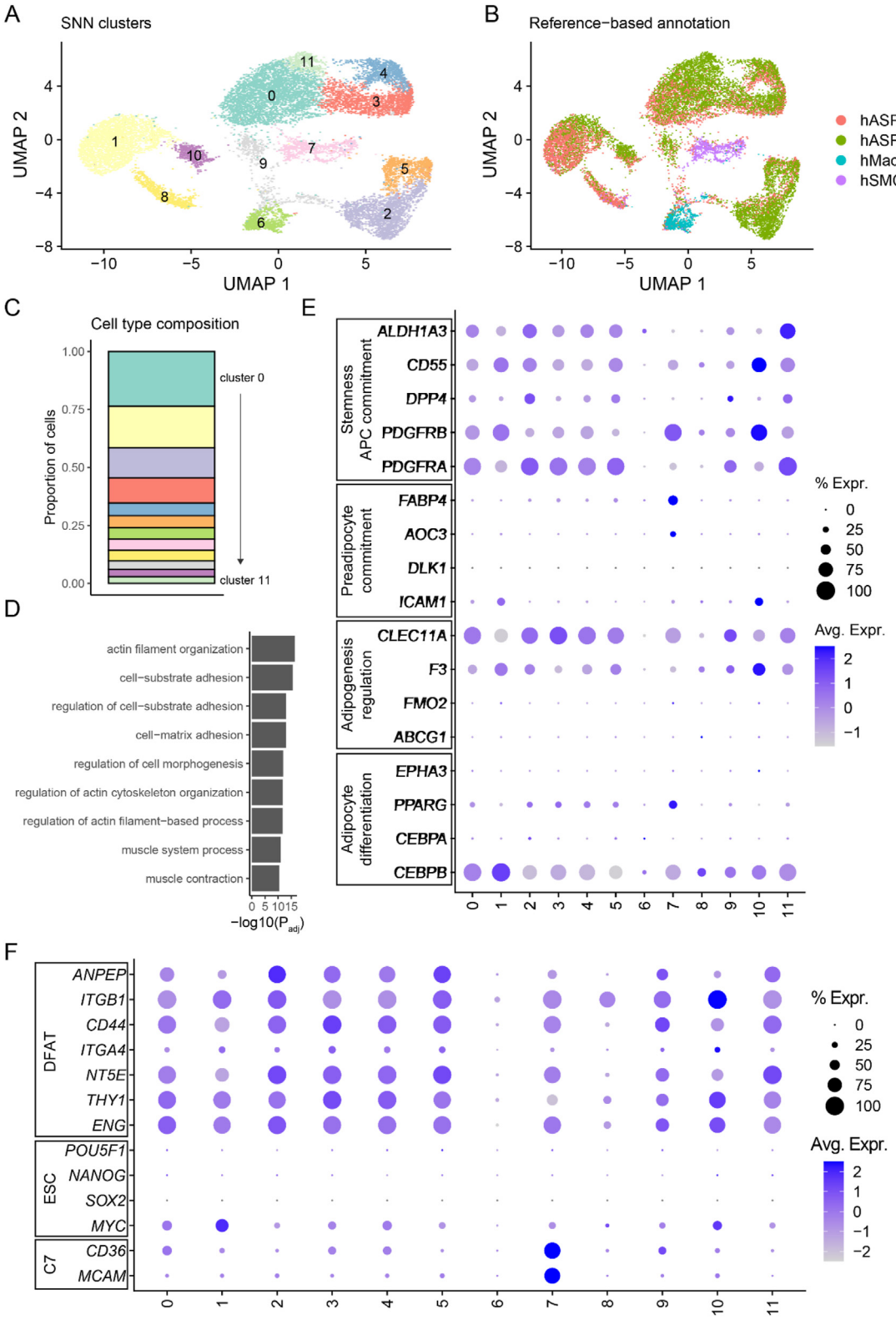

Figure 1: Single-cell RNA-seq clustering and markers for differentiation and commitment in DFAT of 4 individual donors. (A) Unsupervised clustering of 15,731 DFAT isolated from human adipose tissue of four individual donors represented on a UMAP and clustered by shared nearest neighbours (SNN). (B) Reference-based cell type annotation by label transfer. hASPC, human adipose stem and progenitor cell; hMac, human macrophage; hSMC, human smooth muscle cell. (C) Cluster abundance in a bar plot, expressed as proportion of cells per cluster. (color scheme from A) (D) Gene set enrichment analysis for cluster 7 based on marker genes. E) Dot plots comparing the expression of genes reported as markers of stemness and adipose precursor cell commitment, preadipocyte commitment, adipogenesis-regulatory progenitors, and adipocyte differentiation in DFAT. F) Expression of surface markers associated with DFAT, embryonic stem cells (ESC), and cluster 7 (C7). n = 4 independent donors in all panels. (For interpretation of the references to color in this figure legend, the reader is referred to the Web version of this article).

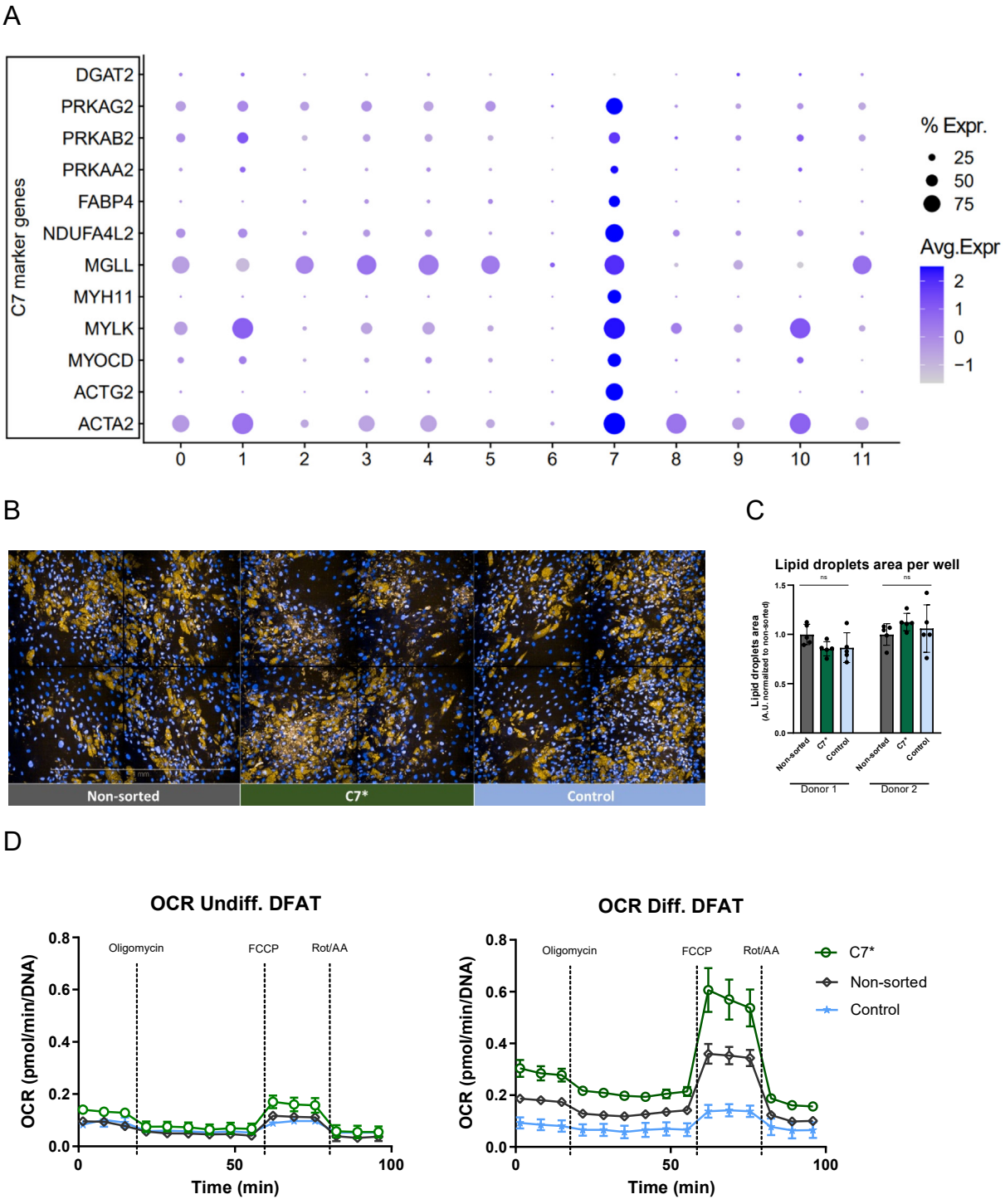

Figure 2: Cluster 7: upregulated genes and metabolic profiling *in-vitro*. (A) Dot plot of genes upregulated in cluster 7 compared to remaining cells. Average normalized expression and percentage of expressing cells of specified genes in different clusters. n = 4 (B) Representative confocal microscopy pictures of DFAT from one human donor sorted by FACS. Lipid droplets of differentiated cells were stained with LipidTOX™ (yellow). DAPI in blue. (C) DFAT from two human donors were sorted, differentiated, and imaged. Automatic software quantification of lipids area per well are expressed as relative to the non-sorted cells. n = 2 biological samples; 5 replicates for each biological sample. (D) OCR of C7*, control and non-sorted cells. Cells were sorted by FACS and OCR was analyzed by Seahorse using the MitoStress Kit. OCR in undifferentiated (left) and differentiated (right) DFAT cells. n = 1; 4 replicates each. (For interpretation of the references to color in this figure legend, the reader is referred to the Web version of this article).

downregulation of genes involved in fatty acid esterification (*DGAT2*) was also found in cluster 7 (Fig 2A). Upregulation of genes involved in energy metabolism indicates a potential for increased metabolic activity in cluster 7 cells, which might play a significant role in the energy balance of human adipose tissue. Therefore, we focused our efforts on further investigating this specific subpopulation.

Two surface markers, CD36 and CD146 (also known as MCAM), were found to have the highest expression in cluster 7 (Fig 1F). CD36 is a

fatty acid transporter and therefore generally found in preadipocytes. However, as CD36 is rather broadly distributed we needed a second marker, CD146, to specifically sort for cluster 7. Therefore, we used a combination of both surface markers for sorting the cells by FACS. These CD36+/CD146+ cells, which resemble cluster 7 (C7*), were compared to CD36-/CD146-cells (control cells) and/or non-sorted cells in terms of their adipogenic and lipid accumulation capacity. For that purpose, C7*, control, and non-sorted DFAT cells went through the adipogenic differentiation protocol and were stained with LipidTOX™ for neutral lipid droplets. Figure 2B—C shows that C7*, control, and non-sorted cells maintain their adipogenic potential and can differentiate and accumulate lipids to a comparable extent. This shows, that C7* indeed is a preadipocyte population that differentiates upon induction, despite having increased expression of muscle cell genes.

Upregulation of genes involved in energy metabolism pointed towards increased metabolic activity in this subpopulation. Therefore, using Seahorse XF analyzer, the oxygen consumption rate (OCR) of C7* was measured and compared to control and non-sorted DFAT cells. As shown in Figure 2D, C7* displays a higher OCR when compared to control and non-sorted cells. The increase in OCR was observed for the basal as well as for the maximal mitochondrial respiration capacity. Importantly, the increase in OCR was found in undifferentiated cells as well as in cells differentiated into adipocytes. As expected, the differences in OCR were stronger when comparing differentiated cells (Fig 2D). These results were replicated in DFAT cells obtained from different human donors (Supp. Fig 4). The scRNA-seq data indicated the possibility of higher metabolic activity in cluster 7. These congruent results demonstrate *in-vitro* the potential of these energy-burning cells and open opportunities for future research.

2.3. Bulk RNA sequencing of differentiated C7* spheroids elucidate upregulation of energy-processing pathways

Our initial scRNA-seq data from preadipocytes was expectedly unable to predict important changes that might occur after adipogenesis and lacked the possibility to integrate it with datasets of human adipocytes. Therefore, we performed bulk RNA sequencing (RNA-seq) of C7* and control DFAT cells from the same donors. These subpopulations were sequenced in regular 2D culture before and after differentiation into adipocytes. In addition, since it has been reported that 3D/spheroid cultures more closely resemble the biology of adipose tissue [21], we generated spheroids of both cell subpopulations and differentiated them before RNA-seq. As expected, the differentiation status accounts for the biggest variation in the gene expression profile of the cells. The differentiated cells in both 2D and 3D formats clustered more closely together than they did with the undifferentiated cells. However, there were also clear differences between the differentiated cells determined by the culture conditions (2D vs 3D) (Supp. Fig 5A-B). In fact, the more prominent differences between C7* and control cells were found when the cells were differentiated as spheroids. Our results also show that growing the cells in 3D culture as spheroids promotes a stronger expression of classical adipocyte-enriched genes (like *PNPLA2*, *PLIN1*, *APOC1*, *FABP4*, *LIPE*, *LEP*, *PPARG*) except for *ADIPOQ*, which was expressed at a comparable level in differentiated 2D and 3D cultures. Interestingly, *LEP* was only expressed in 2D cultured cells after differentiation (Supp. Fig 5C). Hereby, we confirmed the closer resemblance of 3D cultures with actual adipocytes and collected the data to study the transcriptional changes of C7* cells after differentiation that might explain the observed phenotype.

As described above, most of the observed changes in gene expression came from the comparison between undifferentiated vs. differentiated cells. We then focused on the differences between C7* and control cells in the differentiated spheroids (Figure 3A—B). GO annotation identified upregulation in C7* cells of genes involved in adipogenesis (Fig 3C), mitochondrial function (Supp. Fig 6A), oxidative phosphorylation (Supp. Fig 6B), and citric acid cycle (Supp. Fig 6C). Of note, some of the regulated genes in C7* differentiated spheroids had been previously identified by the scRNA-seq approach in the undifferentiated cluster 7 (Supp. Table 2). These data agree with the increased metabolic activity of this subpopulation by demonstrating upregulation of pathways involved in uptake, storage, and oxidation of energetic substrates.

2.4. Evidence for C7 cells in native human white adipose tissue

To determine whether C7-like cells can be identified in native human white adipose tissue, we integrated our present data with our recent meta-analysis of human white adipose tissue sc/snRNA-seq data sets comprising >400.000 cells from 17 cohorts and 83 individuals [22]. As shown in Figure 3, in vitro differentiated C7* cells retained their capacity to differentiate into adipocytes. In line with this, we found that upregulated genes as identified by the bulk sequencing approaches described above were enriched in adipocytes (Figure 4A) in the single cell data. Based on our initial scSeq data, C7 cells were enriched for smooth muscle cell specific genes. Indeed, when comparing these genes with single cell data of native adipose tissue we found them to be enriched in smooth muscle cells and pericytes (Fig 4B). To explore whether cluster 7 resembles endothelial cells identified *in vivo*, we integrated our DFAT scRNA-seq data with the previously published native sn/scSeq data. As C7 cells resembled preadipocytes, but also had characteristics of smooth muscle cells, we specifically integrated our data with all fibroblast and endothelial cells from the meta-analysis. For the integration, we used the same bioinformatic approaches as for the initial analysis. Even after integration with the more complex, native adipose tissue sn/scSeq data, the identified subpopulations (C0—C11) still clustered in a similar and distinct manner: This suggests strong transcriptional states that align well with cell clusters found *in vivo* (Fig 4C). Next, we reclustered the integrated data to see which native adipose tissue cells cluster with C7 cells. After reclustering, we could identify all expected major cell classes. We also identified a cluster which contained the C7 cells (Fig 4D). A comparative expression analysis of original C7 marker genes across all integrated clusters highlights their specificity in C7-like cells (cluster #9, Supp. Fig. 7). When taking a detailed look across included cohorts for the C7-like cells specifically, the original C7 marker genes were evenly distributed (Fig 4E). However, the proportion of C7-like cells varied between ~0.8% and 5% of total fibroblasts and endothelial cells per cohort (Fig 4F). Next, we were interested to understand how the profile of dedifferentiated adipocyte marker genes is influenced by adipogenesis. While the C7* bulk RNA-seq profiles increased with differentiation time, the scRNA-seq C7 profile was reduced on both transcriptome and proteome levels [23] (Fig 4G). Taken together, these data suggest that cells in cluster 7 could represent a unique cell type closely resembling *in vivo* fibroblasts and smooth muscle.

2.5. Abundance and gene signature of C7* cells correlate with important metabolic traits in human subjects

Next, we investigated the possibility of a correlation between the proportion of cells in cluster 7 of DFAT and the body mass index (BMI) of the respective human donor. For that purpose, DFAT were isolated from subcutaneous abdominal adipose tissue from eleven female donors with BMI ranging from 18 to 37 kg/m^2, and the percentage of C7* cells was quantified by FACS (Figure 5A-B). Remarkably, a marked negative correlation was found between the amount of C7*

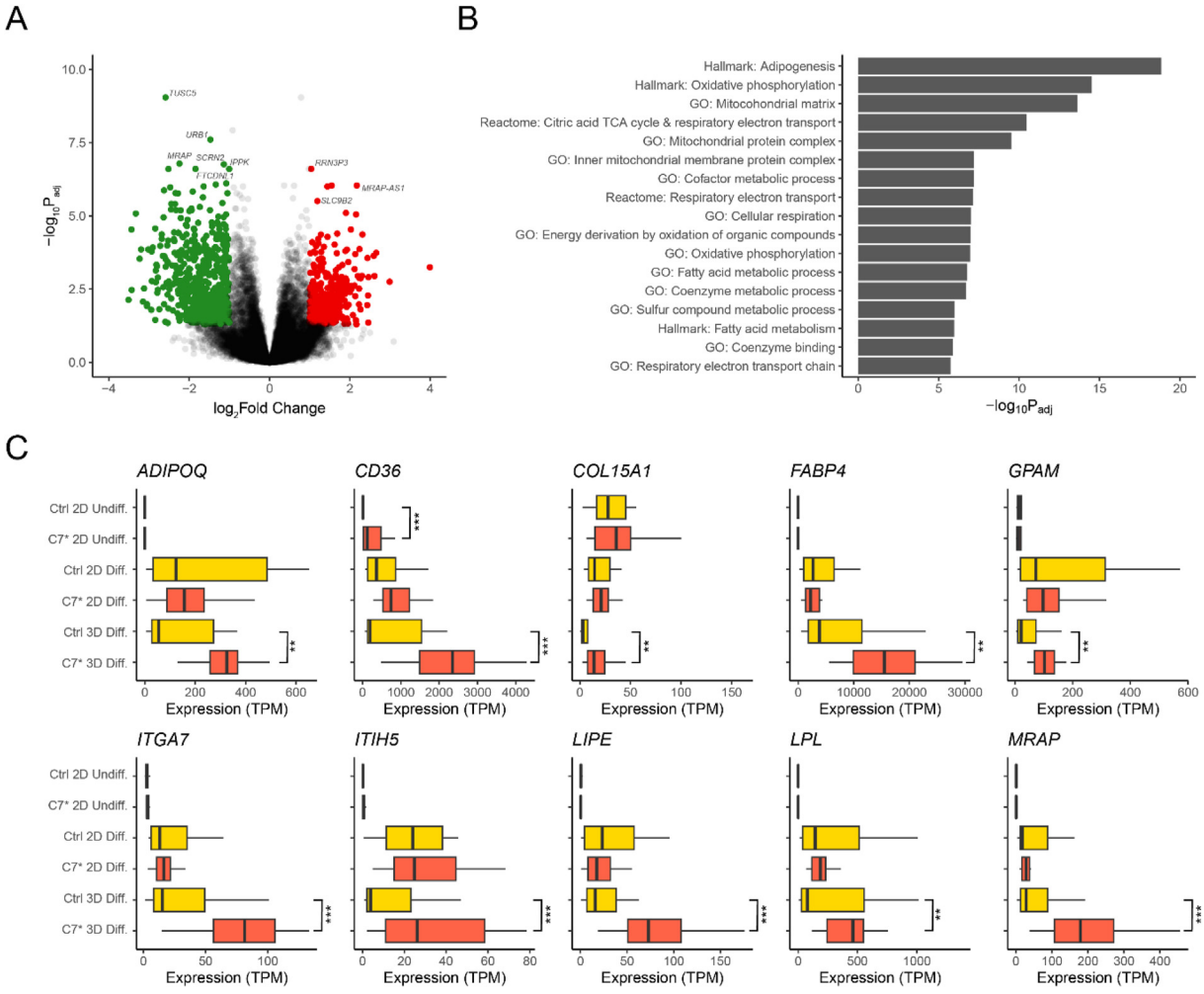

Figure 3: Significantly regulated genes and cellular pathways in spheroids of C7* DFAT cells. (A) Volcano plot illustrating the downregulated (green) and upregulated (red) genes in 3D culture of control cells when compared to C7* using four different donors. A log_2FC threshold of 1 and P_{adj} threshold of 0.05 were used for colouring points. (B) Gene ontology enrichment expressed as the $-log_{10}P_{adj}$ of enrichment of the principal pathways and cellular process in 3D cultured C7* DFAT cells (C) Expression of genes involved in adipogenesis in the specified conditions. Statistically significant differences (limma moderated t test, Benjamini-Hochberg adjusted) between control cells and C7* are indicated by * $P_{adj} < 0.05$, ** $P_{adj} < 0.01$, *** $P_{adj} < 0.001$. n = 4 for all panels. (For interpretation of the references to color in this figure legend, the reader is referred to the Web version of this article).

cells and the BMI of the donor from where the DFAT cells were obtained. These cells reached over 10% prevalence in the donors with the lowest BMI (18 kg/m^2), declined with rising in BMI, and were almost undetectable in samples from obese donors with a high BMI (37 kg/m^2). These findings link an increased abundance of energy-burning cells in the adipose tissue with a low BMI in the respective donor. This was strengthened by comparing the fraction of C7-like cells directly in human adipose tissue from different depots to donor BMI (n = 32) reported in Emont et al., showing increased C7-like cell occurrence with decreasing BMI [3] (Fig 5C).

Furthermore, another translational approach was performed with an over-representation analysis of genes differentially expressed in C7* cells and genes with expression in subcutaneous adipose tissue positively or negatively correlated with 50 continuous clinical parameters in large human cohort (Leipzig Obesity BioBank) of 1759 donors [24–26]. Specifically, we performed hypergeometric tests for overlap of the top 0.5% most up-regulated and most down-regulated genes in C7* compared to control cells in the top 0.5% genes most correlated and anticorrelated genes with each clinical parameter (Fig 5D). The greatest over-representation was observed for genes up-regulated in C7* compared to control cells with genes anti-correlated with the parameters like glycated hemoglobin (HbA1c), body weight, body mass index (BMI), hip circumference, and plasma insulin (Fig 5E). This signal was mainly driven by genes including *TMEM132C*, *AZGP1*, *MAOB*, and *PPP1R1B* (Figure 5F–G). These results demonstrate a correlation between the abundance of this energy-burning cell type and the metabolic fitness of the respective donor.

In summary, this study describes, at the gene expression level, significant and unknown characteristics of DFAT cells regarding their adipogenic, browning and stemness potential. scRNA-seq identified most of the cells as ASPCs and enabled the recognition of a specific subpopulation with muscle-like gene expression signature. This specific subpopulation is characterized by increased oxygen consumption rate and alterations in signaling pathways regulating energy metabolism. Finally, our data demonstrates, not only that this subpopulation is likely to be found in human adipose tissue, but also its clinical significance. Firstly, we found an inverse correlation between the abundance of these cells and the BMI of the donor. And

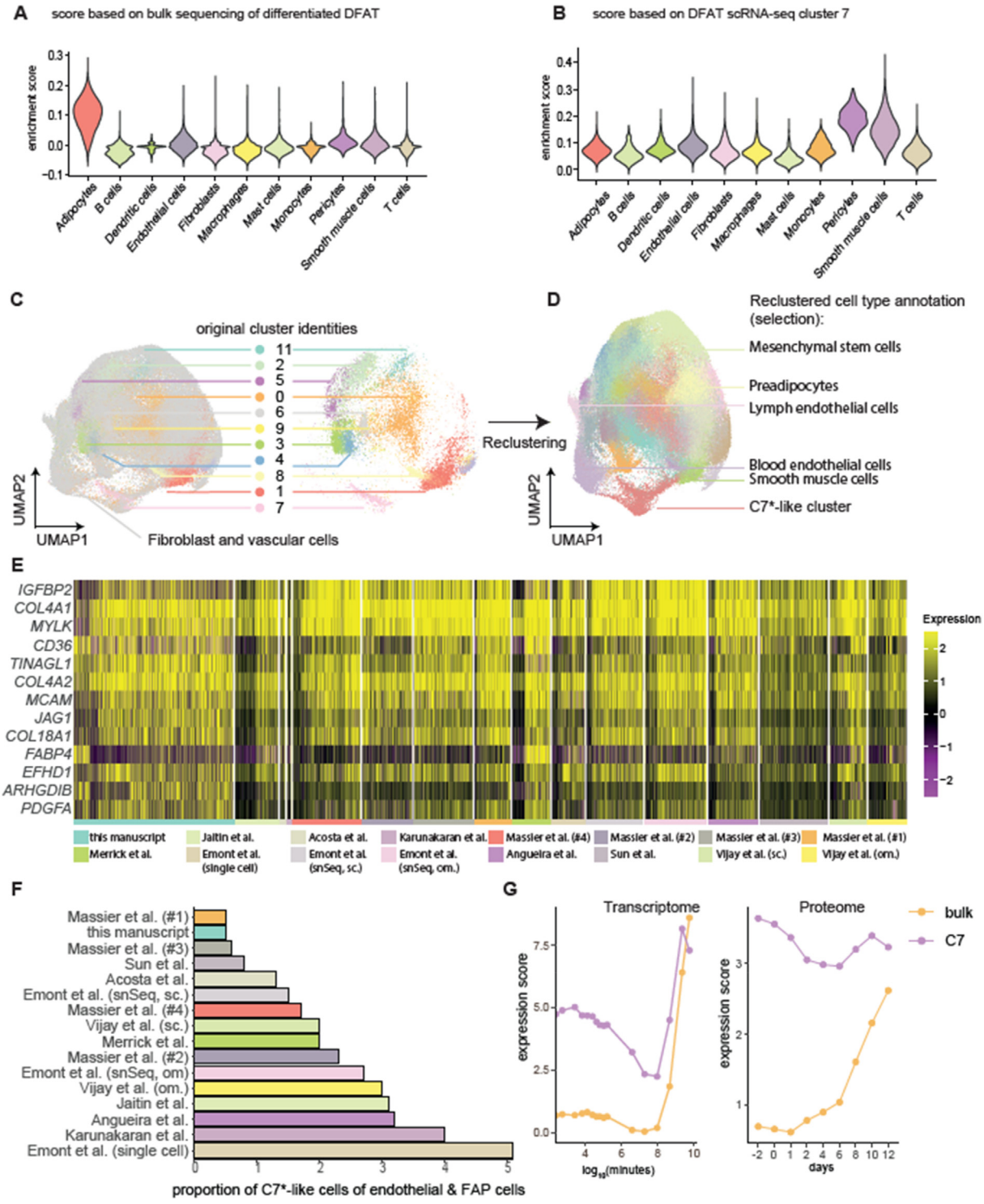

Figure 4: Meta-analysis of cluster 7 in comparison to 17 human snRNA-seq data sets. Enrichment scores calculated based on marker genes of differentiated DFAT bulk RNA sequencing (A) and DFAT scRNA-seq cluster 7 (B) and plotted as violin plots. The results indicate similarity to adipocyte and smooth muscle cell signatures, respectively, when compared to a meta-analysis of 17 human snRNA-seq data sets. C) After integration of our DFAT scRNA-Seq data with endothelial and fibroblast cells of 17 cohorts all clusters can still be distinctively identified; D) Reclustering identifies a cluster of dedifferentiated adipocytes next to other major cell types; E) Heat map showing expression of C7 marker genes in C7-like cells from human adipose tissue sn/scRNA-seq data (17 cohorts, 83 individuals); F) C7* signature is downregulated with adipogenesis on both transcriptional and proteome levels, while marker genes derived from bulk RNA sequencing are increasing.

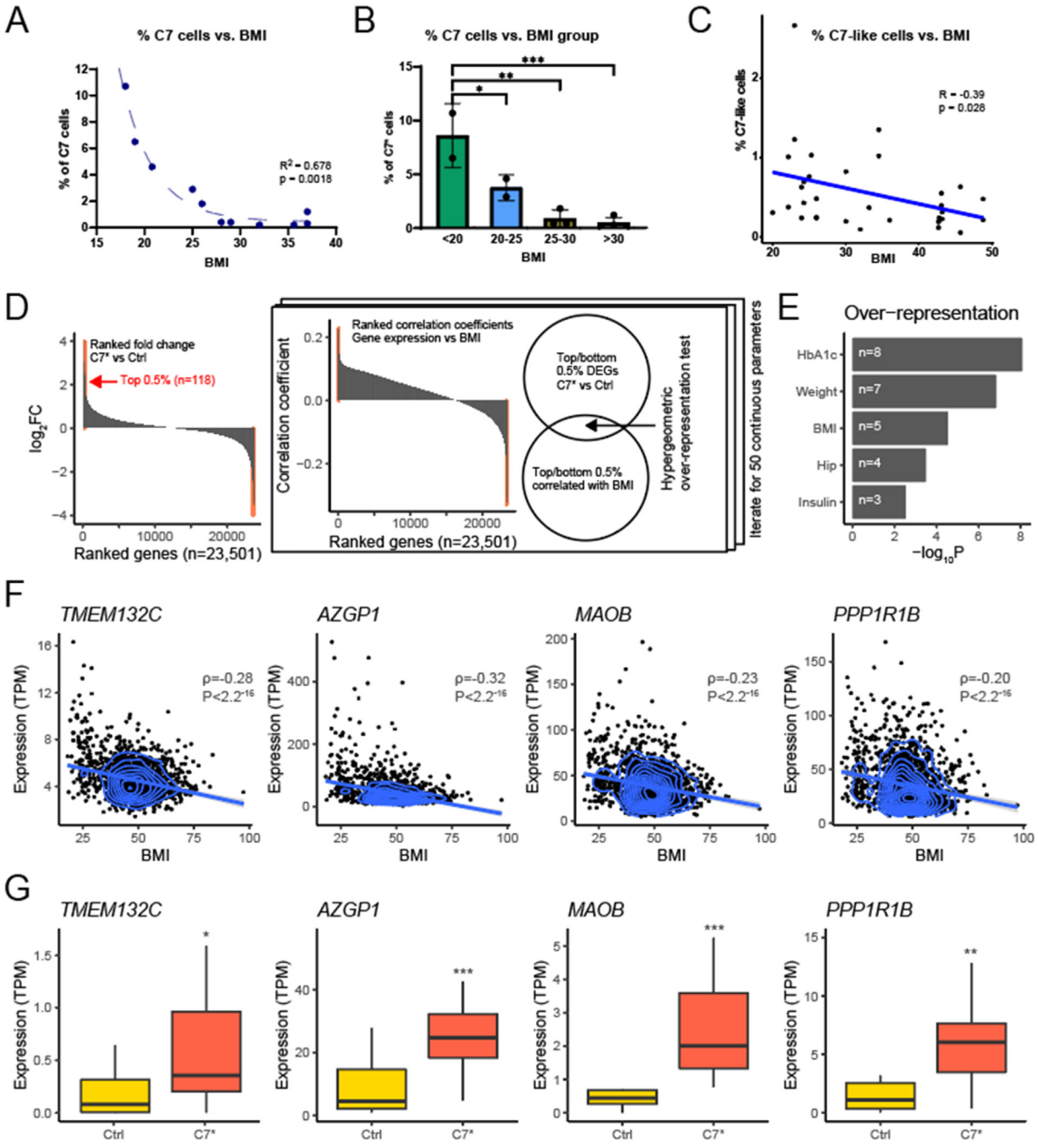

Figure 5: Abundance and gene signature of C7* cells correlate with metabolic traits in humans: (A) Percentage of C7* cells in DFAT obtained from subcutaneous abdominal adipose tissue vs. the BMI of the respective human donor. (B) Data from (A) grouped as different BMI groups. n = 11. (C) Percentage of C7-like cells in adipose tissue from donors with different BMI (n = 32) taken from Emont et al. [3]. (D) Overview of over-representation approach. The 0.5% most differentially expressed genes in C7* cells were compared with the 0.5% genes most correlated with 50 continuous clinical parameters in a human cohort of 1759 donors. (E) Over-representation analysis of genes most strongly inversely correlated with the indicated traits in the set of genes most strongly upregulated in C7* DFAT cells. Values shown are -$\log_{10}$P of a hypergeometric over-representation test. The number of overlapping genes is indicated in each bar. (F) Correlation between the expression of the selected genes in subcutaneous adipose tissue and the body mass index (1759 donors). Pearson correlation coefficients are indicated in each case. (G) Expression of the indicated genes in the respective cell populations in 3D culture (n = 15–16). Statistically significant differences (limma moderated t test, Benjamini-Hochberg adjusted) are indicated by * $P_{adj} < 0.05$, ** $P_{adj} < 0.01$, *** $P_{adj} < 0.001$.

second, the gene expression in this subpopulation inversely correlates to important metabolic parameters in a large human cohort. This demonstrates the significance of our results and opportunities arise for new therapeutic approaches aiming to increase or stimulate this specific subpopulation to promote energy expenditure and metabolic fitness.

3. DISCUSSION

Currently, there is a growing interest in the characterization of adipose tissue and precursor cells at the single cell level. Adipocytes and their progenitors have been demonstrated to be plastic and dynamic, significantly impacting adipose tissue homeostasis and the response to

therapeutic interventions. Here, we profile DFAT cells, a model of induced pluripotent stem cells with potential for disease treatment and regenerative medicine. scRNA-Seq characterized most of the DFAT as stem and precursor cells, showing low expression of genes reported as indicators of commitment. However, we found significant expression of genes involved in adipogenesis and normally expressed in more committed or mature adipocytes. We show that markers for commitment and adipogenesis were not completely aligned with previously published information, demonstrating that such markers are still debatable due to donor-to-donor variability, differences in the origin of the adipocyte precursor cells, or culture duration [3,15,27]. Although we cannot exclude artifacts due to cell preparation, our cells behave as reported, regarding the de- and re-differentiation potential, and express DFAT typical genes shown in previous publications [6]. Certain surface markers have been reported to be found on DFAT cells including *ANPEP* (*CD13*), *ITGB1* (*CD29*), *CD44*, *ITGA4* (*CD49d*), *NT5E* (*CD73*), *THY1* (*CD90*), and *ENG* (*CD105*) [6]. This is in line with our findings, as the majority of these surface markers are ubiquitously expressed in our DFAT cells. On the other hand, we can only detect MYC as a marker associated with embryonic stem cells, whereas other reported markers, such as *POU5F1* (*OCT4*), *SOX2*, and *NANOG* [6], remained undetected. Such markers are relevant to sustain pluripotency, but also decrease significantly after two weeks in culture [6] which could explain the low expression of these genes in our DFAT, as our cells were cultured over a two-weeks period. Overall, these findings support the variability of precursor cells and the uniqueness of DFAT cells. Our results indicate that DFAT cells are non-committed adipocyte precursor cells with multipotency potential.

Moreover, clustering of DFAT cells allowed us to identify a specific subpopulation with a gene signature related to muscle. This cell cluster shows no alterations in pathways regulating adipogenesis, and it was effectively induced into differentiation and lipid accumulation. This subpopulation (C7*), designated by the expression of *CD36* and *CD146*, demonstrated an increased oxygen consumption rate, not only before, but also after differentiation. Long et al. describe a population of mouse adipose tissue smooth muscle-like cells (SMCs) which can give rise to thermogenic beige adipocytes [28]. The SMCs described in the publication express Myh11 and Acta2, and do not express Prdm16 and Ppargc1 prior to differentiation. Similarly, C7 cells from our study express MYH11 and ACTA2, but not PRDM16 and PPARGC1. Thus, we surmise that C7 cells are similar to the SMCs described in the cited publication [28]. This shows that these cells are intrinsically more metabolically active, independent of the differentiation state. Since high energy expenditure in adipocytes could generate a negative energy balance, this might be useful for the treatment of obesity and comorbidities.

In addition, due to technical difficulties when dealing with lipid-loaded adipocytes, the scRNA-seq data was limited to undifferentiated cells. This issue was addressed by using bulk RNA-seq, which offered a clearer picture of this subpopulation after differentiation. From the bulk RNA-seq approach, we also gained significant knowledge concerning the biology of this subpopulation and the behavior of DFAT in different *in-vitro* systems. As previously reported, we showed that the induction of differentiation of adipose precursor cells is more efficient in 3D cultures [21,29]. This is important for the translatability of *in-vitro* experiments because they more closely reflect the biology of actual adipose tissue. Furthermore, our approach facilitates large scale experimentation due to the low number of cells needed and the quality of the low-input sequencing method. The bulk sequencing data confirmed the upregulation of genes involved in the handling and consumption of energy after differentiation and clarified some of the pathways involved in the observed phenotype, such as mitochondrial function, oxidative phosphorylation, and citric acid cycle. These gene sets are likely responsible for the increase in oxygen consumption rate in adipocytes and specifically in the C7* subpopulation.

The comparison of samples obtained from different donors highlights the translational relevance of this C7* subpopulation in adipose tissue biology. We demonstrated that not only are these cells found in human adipose tissue, but also an inverse correlation between the fraction of these cells and the BMI of the donor. We also demonstrated significant correlations between our *in-vitro* findings and subcutaneous human adipose tissue regarding important metabolic parameters related to weight and glucose control. These findings raise two important points. Firstly, DFAT cells dedifferentiate and recover their proliferative ability, however, they retain traits from the donor which is later reflected in the transcriptome and metabolic profile of the cells. Secondly, and perhaps more clinically significant, it seems plausible that having more of these highly energetic cells might help to reduce the body weight of the respective human subject. However, we cannot exclude that this process works the other way around, such that maintaining a low body weight favors the expansion of this subpopulation.

We further confirm previously described genes modulating energy metabolism, but more importantly, we report sets of genes which are potential targets for future studies in the field of obesity as modulators of energy expenditure. This is underlined by genes that are clearly upregulated in either our C7 DFAT subpopulation and/or the 3D spheroids from C7*, such as melanocortin 2 receptor accessory protein (*MRAP*) and alpha-2-glycoprotein 1, zinc-binding (*AZGP1*). Overexpression of *MRAP* decreases adiposity and body weight gain in high-fat diet fed mice, along with an increased expression of genes involved in mitochondrial fatty acid oxidation and thermogenesis in adipose tissue [30]. Moreover, deletion of MRAP results in severe obesity in mice, and human rare heterozygous variants result in severe obesity [31,32]. Another gene, *AZGP1*, also upregulated in differentiated C7* spheroids, was shown to play an important role in regulating energy homeostasis and lipid metabolism. In adipose tissue of humans, *AZGP1* expression is downregulated in obesity and obesity-related insulin resistance [33]. *AZGP1* KO inhibited body weight loss in mice upon cold induced stress. *In-vitro* overexpression of *AZGP1* in adipocytes enhanced expression of markers for browning and mitochondrial biogenesis [34,35]. Furthermore, *AZGP1* overexpression in POMC neurons reduced food intake and increased energy expenditure whereas deletion of *AZGP1* demonstrates the opposite [36]. Overall, animal models as well as human studies summarized by Banaszak et al. highlight the important role of *AZGP1* in reducing obesity and maintaining insulin sensitivity [37]. On the other hand, *MOAB* was also upregulated in our C7* cells, although the literature rather reports a reduction of body weight and fat accumulation upon inhibition of *MOAB* [38,39]. Furthermore, disruption of glucose or insulin signaling can lead to complications upon obesity. We identified genes that are important in this regulation, such as *TUSC5* and *PPP1R1B*. *TUSC5* is highly expressed in white and brown adipocytes and its expression increases throughout adipocyte maturation [40,41]. *TUSC5* is a regulator of insulin stimulated glucose transport as it colocalizes with *GLUT4* and KO mice show impaired glucose disposal [42]. The fact that it is regulated by *PPARG* also indicates a role of *TUSC5* in adipocyte metabolism. However, even though *TUSC5* might play a significant role in glucose control, the fact that no difference was observed in *TUSC5* expression between lean and obese subjects leaves the role of *TUSC5* in obesity equivocal [41]. *PPP1R1B*, on the other hand, was shown to regulate glycogen associated protein phosphatase 1 (*PP1*)

activity, suggesting a role of *PPP1R1B* in insulin signaling [43]. Taken together, these findings show that there is a modulation of a set of genes in this subpopulation, which leads to increased energy expenditure and improved glucose and insulin regulation and might potentially be used to treat obesity and obesity-related comorbidities, such as insulin-resistance.

In summary, finding ways to promote proliferation or activation of this subpopulation, as well as modulating one or multiple genes it expresses, can have important therapeutic potential in the field of obesity. In fact, transplantation of adipose tissue, to boost the mass of energy-burning cells, has been proposed for treatment of patients with obesity and it has already been tested preclinically *in-vivo* [8]. Different approaches, including gene therapy and tissue transplantation, have shown to be feasible and perhaps an option for medical treatments [8,44–46]. By identifying and characterizing this subpopulation of DFAT cells, opportunities arise for future applications in the treatment of obesity and comorbidities.

4. MATERIALS AND METHODS

4.1. Human adipose tissue samples for dedifferentiated adipocytes isolation

Subcutaneous abdominal adipose tissue from human donors was collected under a valid informed consent by the Stiftung Human Tissue Cell Research c/o Zentrum für Leberzellforschung, Klinik der Universität Regensburg. This informed consent, under which the tissue was collected, was provided to Boehringer Ingelheim. The human tissue was then provided to Boehringer Ingelheim under a frame service agreement. For each donor, several parameters were reported including body mass index (BMI), age and gender. Around 30–60 g of abdominal adipose tissue were collected during surgery and placed in dry ice until further processing.

4.2. Dedifferentiated adipocytes preparation

The day after collection, the adipose tissue was treated as previously described [47,48]. It was cut into small pieces and blood vessels and connective tissue were removed. Small pieces of adipose tissue were digested for 10 min at 37 °C with 1 mL of collagenase II (1 mg/mL) per gram of tissue. The tissue was then filtered through gauze and the collagenase reaction stopped by the addition of FBS containing medium. The phases were allowed to separate for 1–2 h, afterwards, the floating adipocytes in the supernatant were carefully collected for generation of DFAT.

DFATs are grown by completely filling a cell culture bottle with medium containing the adipocytes and placing it upside down for a week at 37 °C and 5% CO_2. After that period, cells lose their lipid droplets and start proliferating. Therefore, the culture bottle can be placed normally and medium changed.

4.3. Cell culture and differentiation

After isolation DFAT were maintained in DMEM F-12 medium (BIO WITTHAKER. Ref: BE12-719F) containing 15% FBS (Biol Industries. Ref: 04-001-1A) and 1% Anti–Anti (Gibco. Ref: 15240-062). Medium was changed every 2 days and cells were not allowed to reach confluency.

Differentiation of preadipocytes into mature adipocytes was induced with Omental Adipocyte Differentiation Medium (Zenbio. Ref: OM-DM-500) for one week and then Omental Adipocyte Maintenance Medium (Zenbio. Ref: OM-AM-500) for the week after. For OCR experiments, DFAT cells (20000 cells/well) were differentiated in a 96-well Seahorse XF plate using the same differentiation medium.

4.4. Single-cell RNA-sequencing

For scRNA-seq, DFAT from four human donors in passage 2 were washed with PBS and detached with 1xTrypsin in PBS/EDTA (4 min at 37 °C) and gently handled with wide-bore 1000 μL tips. Cells were resuspended in PBS with 0.5% BSA and 2U/uL RNAse inhibitor and placed on ice. Cell concentration, viability (>90%), and aggregates (<5%) were determined with the NucleoCounter NC-3000 (Chemometec) cell counter. All single cell suspensions passed quality criteria with cell viability >95% (Mean: 96.9% ± 0.46 SEM) and cell aggregates <4% (Mean: 2.2% ± 0.34 SEM). Single-cell RNA-seq libraries were generated with the Chromium Next GEM Single Cell 3′ Kit v3 (10x Genomics) according to the manufacturer's instructions. Briefly, a targeted cell recovery of 5000 cells was employed and cell capture conducted with the Chromium controller followed by reverse transcription as per manufacturer's instructions (10x Genomics). After an additional bead clean-up, the cDNA yield ranged from 60 ng to 415 ng (Mean: 280 ng ± 29.5 SEM). A total of 50 ng of cDNA was used for the scRNA-seq library preparation of single indexed libraries with the addition of a final 1x SPRISelect bead clean-up (Beckman Coulter) to ensure full removal of primer and adaptor dimers prior to the final elution for gene expression libraries. Libraries were quantitatively and qualitatively assessed using the 1x dsDNA kit on the Qubit 4 Fluorometer (ThermoFisher) and the High Sensitivity NGS Fragment 1–6000 bp kit on a 48-channel Fragment Analyzer (Agilent), respectively. Gene expression libraries were 494 bp ± 4.2 SEM with a yield of 59.3 nM ± 3.8 SEM. Libraries were normalized, pooled, spiked in with 5% PhiX Control v3 and clustered on a cBot instrument with the HiSeq 3000/4000 Paired-End Cluster Kit (Illumina). The Flow Cell was sequenced on an Illumina HiSeq 4000 with the following run parameters: Rd1. 28 bp, Rd 2. 8 bp, Rd 3. 91 bp. We reached an average mean depth of 49746 ± 2113 SEM pass-filter reads per cell. Before any quality filtering, we detected 4796 cells per sample with a reported average of 4690 ± 101.9 SEM genes per cell.

4.5. Single-cell RNA-sequencing data analysis

4.5.1. Process raw fastq reads of 10X scRNA-seq data

We used STARSolo (v 2.7.3a [49]) to map the raw fastqs, demultiplex cell barcodes, and generate a count matrix with GTF annotation downloaded from Ensembl (v86 [50]). The count matrix was then loaded into Seurat [51] for downstream analyses, including basic QC, normalization, identification of variable genes, clustering and batch correction, and integration. Briefly, we removed cells with fewer than 300 or more than 8000 genes detected, and with more than 50% of UMIs derived from mitochondrial RNAs. We used Seurat function NormalizeData to normalize and log-transform raw UMI counts. We regressed out the number of UMIs per cell and the percentage of mitochondrial RNAs as confounders individually and scaled the resulting residuals as input into the computation of Principal Components (PCs). The top 50 PCs were selected for graph-based clustering with a resolution parameter 0.6, which has been implemented in FindNeighbors and FindClusters functions of the Seurat package.

4.5.2. Integrative analysis of scRNA-seq datasets derived from multiple conditions/donors

As we observed batch effects in multiple scRNA-datasets, we performed an integrative analysis to remove batch effects before cell clustering, so that the same cell types could be clustered together. We used FindIntegrationAnchors and IntegrateData functions in

Seurat on the top 20 CCAs to integrate multiple scRNA-seq datasets. The UMAP of integrated datasets was computed with the RunUMAP function.
Gene set enrichment analysis was performed by first finding enriched genes in cluster 7 using FindAllMarkers from Seurat (minimum % 25, log fold change threshold 0.25), yielding 452 enriched genes. Enrichment was measured using enrichGO with Benjamini-Hochberg P value adjustment, a P value cutoff of 0.01, and a q value cutoff of 0.05.

4.5.3. Meta-analysis

Scores to compare marker gene profiles to existing, integrated snSeq data was calculated using the AddModuleScore function in Seurat v4.3.0, which calculates the mean expression of the provided gene list and is corrected using the expression of control feature sets [52]. Marker genes were selected based on adjusted p-value below 0.05. Integration with endothelial and fibroblast cells was performed as described above. Scores for adipogenesis were calculated as average expression of marker genes over background expression of all genes. Heatmap to show expression of C7 marker genes across clusters and cohorts was generated in Seurat using the DoHeatmap function.

4.5.4. Correlation

BMI information was available for the snSeq and scSeq data published by Emont et al. [3]. To perform correlation analysis with BMI, we calculated the proportion of C7-like cell per subject and correlated it with reported BMI values using Spearman's rho. SnSeq and scSeq from adipose tissue and SVF of omental and subcutaneous fat from 32 patients were used.
To compare with the Emont et al. dataset [3], we used a reference mapping approach to integrate our scRNA-seq dataset. We selected only Caucasian individuals from reference dataset for this comparison. We identified anchor cells between our scRNA-seq dataset and the reference dataset in a shared low-dimensional space based on overlapping high-variable features. These anchor cells were then used to project our scRNA-seq dataset onto the reference, transferring cell type labels and metadata to the query dataset.

4.6. Low-input mRNA-seq (bulk RNA sequencing)

114 total RNA samples from FACS sorted subcutaneous adipose tissue were assessed both qualitatively and quantitatively using the High Sensitivity Total RNA 15 nt Analysis DNF-472 on a 96-channel Fragment Analyzer (Agilent). Total RNA yield ranged from 0.04 ng to 61.8 ng (Mean: 14.06 $\pm$ 0.73 SEM). RIN value for most samples was $>$7.5, with only 9 samples having a RIN $<$7.5, with ranging RIN values from 3.0 to 7.1 (Mean: 9.2 $\pm$ 0.12 SEM).
Up to 3 ng of total RNA was used for cDNA synthesis with the SMART-seq® v4 Ultra Low Input RNA kit (Takara Bio). 10 cDNA amplification cycles were employed and after clean-up an average cDNA yield of 11.7 ng $\pm$ 0.64 SEM was obtained, ranging from 2.4 to 49.2 ng. To generate final sequencing libraries up to 5 ng of cDNA were used with the Tagmentation-based DNA prep kit and the IDT®DNA/RNA Dual Indexes set B and C, both Illumina. Indexing PCR was performed with 12 cycles and final library was eluted in 30 μL of EB Buffer (Qiagen).
Low input libraries were quantified using the fluorescence-based High Sensitivity dsDNA Quanti-iT Assay Kit (ThermoFisher) using a Synergy HTX microplate reader (BioTek) and qualitatively assessed for size and adapter dimer presence by the High Sensitivity NGS Fragment 1—6000 bp Kit on a 96-channel Fragment Analyzer (Agilent). In average, libraries were 478 bp $\pm$ 3.11 SEM long and 73.06 nM $\pm$ 1.61 SEM in molarity. One library was dropped out due to low yield.
A total of 113 libraries were normalized on a MicroLab STAR (Hamilton), pooled and spiked in with 1% PhiX Control v3 (Illumina). The library pool was subsequently sequenced on an Illumina NovaSeq 6000 using an S4 Reagent Kit v1.5 (Illumina) with the following run parameters: Rd1:101bp, Rd2: 10bp, Rd3: 10bp, Rd4:101bp, reaching an average depth of 53.3 $\pm$ 0.66 million Pass-Filter reads per sample.
Sequencing reads were processed as previously described [53]. Differential expression analysis was performed on the mapped counts derived from featureCount using limma/voom [54,55].

4.7. Isolation of C7* DFAT cells by FACS

DFAT cells were allowed to grow without reaching confluency. Cells were washed twice with PBS/EDTA and detached with 1xTrypsin in PBS/EDTA (5 min at 37 °C). Cells were counted and centrifugated at 400 G for 5 min and resuspended in PBS with 0.1% BSA containing the antibodies or the isotypes control. The incubation occurred at a concentration of 1 $\times$ 10^6 cells per 100 μL at 4 °C for 1 h in the dark in a double platform shaker. 20 μL of APC Mouse Anti-Human CD36 antibody (BD Pharmingen #550956. Clone CB38) or APC Mouse IgM, κ Isotype Control (BD Pharmingen #555585. Clone G155-228) plus 5 μL of BV421 Mouse Anti-Human CD146 antibody (BD Horizon #564325. Clone P1H12) or BV421 Mouse IgG1, κ Isotype control (BD Horizon #562438. Clone X40) were used per 100 μL of cells suspension. Cells were washed twice with PBS/EDTA and resuspended in PBS 0.1% BSA before sorting with the BD FACS Aria IIu (BD Biosciences) or SONY (LE-MA900CP). A 2.0 FSC ND filter was used and the FSC, SSC and fluorescence were set with corresponding isotype controls as follows: firstly, the cells incubated with APC Mouse IgM κ Isotype Control and BV421 Mouse IgG1 κ Isotype control were used to plot the side scatter area (SSC-A) against the forward scattered light area (FSC-A) and generate a gate to select the cells according to size and granularity. Then, same control cells were used to generate the gates with low fluorescence (CD36-CD146-in quadrant Q3-1) and high fluorescence (CD36+CD146+ in quadrant Q2-1) using the lasers 405 nm (for Brilliant Violet 421) and 647 nm (for APC). Graphical representation of gating strategy for isotype control and sorted cells are shown in Supp. Figure 8A-B, respectively. Cells were sorted by purity and non-single cells were automatically discarded. CD36+/CD146+ (C7*), control and non-sorted cells were collected in different tubes and plated accordingly for further experiments.

4.8. Human adipose tissue samples in the LOBB cohort and over-representation analysis

RNA-seq data from subcutaneous adipose tissue of a cross-sectional cohort from the Leipzig Obesity BioBank (LOBB, n = 1759 donors) was used [26]. The LOBB is a collection of human adipose tissue samples, serum/plasma and associated data that was created to extend the knowledge of obesity and related diseases (https://www.helmholtz-munich.de/en/hi-mag/cohort/leipzig-obesity-bio-bank-lobb). Donors of the LOBB span a wide range of age, BMI and include individuals with cardiometabolic diseases. AT samples were collected during elective laparoscopic abdominal surgery as previously described [24] and laboratory measurements of metabolic parameters and body composition were obtained, as detailed before [25]. The Pearson correlation of expression of each gene with each of 50 continuous parameters (body mass index, weight, HbA1c, etc.) was computed. Only genes in common between the expression data from the human donors and from the sorted cells were retained for further analysis (23501 genes). The highest and lowest 0.5% of Pearson correlation coefficients (n = 118) were overlapped with the top 0.5% highest and lowest $\log_2$Fold Change of C7* cells compared to control

cells. A hypergeometric test was used to compute the P value of each overlap.

RNA-sequencing (RNA-seq; rRNA-depleted, single-end) data from the LOBB cohort were generated based on a SMARTseq protocol [56]. In brief, RNA enrichment and reverse transcription were conducted with oligo (dT) and TSO primers. cDNA amplification was carried out with ISPCR primers, and cDNA was processed with Tn5 using the Nextera DNA Flex kit. RNA libraries were sequenced on a Novaseq 6,000 instrument at the Functional Genomics Center Zurich (FGCZ), Switzerland.

The raw reads were adapter trimmed and checked for sufficient quality by applying Fastp (v0.20.0) [57], permitting a minimum read length of 18 nts and a quality cut-off of 20. Aligned to the human reference genome (GRCh38.p13), gene level expression quantification (gene model definition from GENCODE release 32) was carried out using Kallisto (v0.46) [58]. Samples with more than 20 million read counts were downsampled to 20 million read counts using the R package ezRun (v3.14.1; https://github.com/uzh/ezRun). Data were homoscedastically normalized with respect to library size using the variance-stabilizing transformation implemented by DESeq2 (v1.32.0) [59]. To effectively neutralize the effects of *in-vitro* RNA degradation, normalized counts were calibrated with transcript integrity numbers (TINs) [60]. TINs were estimated using the R package RSeQC (v4.0.0) [61]. Finally, the normalized data were adjusted for the gender and age batches.

4.9. Staining and imaging

For staining, the cells were fixed with 3.7% formaldehyde for 30 min at RT, then washed and permeabilized with 0.2% Triton X-100 for 15 min at RT. Cells were washed and then blocked with 2% BSA. The day after, the cells were stained with Hoechst (1 μM) (Life Technologies H3570) for 30 min at 37 °C and then washed. Directly after, they were stained with Cellmask Green stain (1:50000) (Invitrogen H32714), and LipidTOX red neutral lipid stain (1:500) (Invitrogen H34476) for 30 min at RT. Pictures were taken in Opera Phenix (PerkinElmer).

4.10. Oxygen consumption rate measurement with Seahorse XFe 96

Oxygen consumption rate was measured on the Seahorse XFe 96 Extracellular Flux Analyzer using the Seahorse XF Cell Mito Stress Test Kit (#103015-100) as specified by the manufacturer. Oligomycin (2 μM), Carbonyl cyanide-4 (trifluoromethoxy) phenylhydrazone (FCCP) (1 μM), and Rotenone/Antimycin (0.5 μM) were used for the assay.

CRediT AUTHORSHIP CONTRIBUTION STATEMENT

Jonathan Trujillo-Viera: Conceptualization, Data curation, Investigation, Methodology, Writing — original draft, Writing — review & editing, Visualization. **Mona C. Wittmann:** Conceptualization, Data curation, Investigation, Methodology, Writing — original draft, Writing — review & editing, Visualization. **Daniel Lam:** Data curation, Formal analysis, Visualization, Writing — original draft, Writing — review & editing, Methodology. **Yang Shen:** Data curation, Formal analysis, Methodology. **Adhideb Ghosh:** Conceptualization, Data curation. **Falko Noé:** Data curation, Investigation. **Anne Hoffmann:** Data curation, Investigation. **Coralie Viollet:** Conceptualization, Investigation. **Alec Dick:** Conceptualization, Investigation. **Matthias Blüher:** Conceptualization, Supervision, Writing — review & editing. **Jiawei Zhong:** Data curation, Formal analysis, Investigation. **Lucas Massier:** Conceptualization, Data curation, Formal analysis, Writing — review & editing. **Christian Wolfrum:** Conceptualization, Supervision. **Holger Klein:** Conceptualization, Supervision. **Heike Neubauer:** Conceptualization, Supervision, Writing — review & editing. **Bradford Hamilton:** Conceptualization, Supervision, Writing — review & editing.

DECLARATION OF COMPETING INTEREST

The authors declare that they have no known competing financial interests or personal relationships that could have appeared to influence the work reported in this paper.

DATA AVAILABILITY

Data will be made available on request.

APPENDIX A. SUPPLEMENTARY DATA

Supplementary data to this article can be found online at https://doi.org/10.1016/j.molmet.2025.102161.

REFERENCES

[1] Hu T, Chitnis N, Monos D, Dinh A. Next-generation sequencing technologies: an overview. Hum Immunol 2021;82:801—11.

[2] Maniyadath B, Zhang Q, Gupta RK, Mandrup S. Adipose tissue at single-cell resolution. Cell Metab 2023;35:386—413.

[3] Emont MP, Jacobs C, Essene AL, Pant D, Tenen D, Colleluori G, et al. A single-cell atlas of human and mouse white adipose tissue. Nature 2022;603:926—33.

[4] Vijay J, Gauthier M-F, Biswell RL, Louiselle DA, Johnston JJ, Cheung WA, et al. Single-cell analysis of human adipose tissue identifies depot- and disease-specific cell types. Nat Metab 2020;2:97—109.

[5] Shen JX, Couchet M, Dufau J, Barbosa T, Ulbrich MH, Helmstädter M, et al. 3D adipose tissue culture links the organotypic microenvironment to improved adipogenesis. Adv Sci 2021;8:2100106.

[6] Liang Z, He Y, Tang H, Li J, Cai J, Liao Y. Dedifferentiated fat cells: current applications and future directions in regenerative medicine. Stem Cell Res Ther 2023;14:207.

[7] Côté JA, Ostinelli G, Gauthier M-F, Lacasse A, Tchernof A. Focus on dedifferentiated adipocytes: characteristics, mechanisms, and possible applications. Cell Tissue Res 2019;378:385—98.

[8] Dani V, Yao X, Dani C. Transplantation of fat tissues and iPSC-derived energy expenditure adipocytes to counteract obesity-driven metabolic disorders: current strategies and future perspectives. Rev Endocr Metab Disord 2022;23:103—10.

[9] Robin LRV, Roncari DAK. Complete differentiation of adipocyte precursors. Cell Tissue Res 1978;195:317—29.

[10] Gao H, Volat F, Sandhow L, Galitzky J, Nguyen T, Esteve D, et al. CD36 is a marker of human adipocyte progenitors with pronounced adipogenic and triglyceride accumulation potential. Stem Cell 2017;35:1799—814.

[11] Machado SA, Pasquarelli-do-Nascimento G, Silva DS, Farias GR, Santos I, Baptista LB, et al. Browning of the white adipose tissue regulation: new insights into nutritional and metabolic relevance in health and diseases. Nutr Metab 2022;19:61.

[12] Lefterova MI, Haakonsson AK, Lazar MA, Mandrup S. PPARγ and the global map of adipogenesis and beyond. Trends Endocrinol Metabol 2014;25:293—302.

[13] Xue H, Wang Z, Hua Y, Ke S, Wang Y, Zhang J, et al. Molecular signatures and functional analysis of beige adipocytes induced from in vivo intra-abdominal adipocytes. Sci Adv 2018;4:eaar5319.

[14] Shan B, Barker CS, Shao M, Zhang Q, Gupta RK, Wu Y. Multilayered omics reveal sex- and depot-dependent adipose progenitor cell heterogeneity. Cell Metab 2022;34:783—799.e7.

[15] Merrick D, Sakers A, Irgebay Z, Okada C, Calvert C, Morley MP, et al. Identification of a mesenchymal progenitor cell hierarchy in adipose tissue. Science 2019:364.
[16] Zachara M, Rainer PY, Hashimi H, Russeil JM, Alpern D, Ferrero R, et al. Mammalian adipogenesis regulator (Areg) cells use retinoic acid signalling to be non- and anti-adipogenic in age-dependent manner. Embo J 2022;41:e108206.
[17] Hudak CS, Gulyaeva O, Wang Y, Park S, Lee L, Kang C, et al. Pref-1 marks very early mesenchymal precursors required for adipose tissue development and expansion. Cell Rep 2014;8:678–87.
[18] Zhang Q, Shan B, Guo L, Shao M, Vishvanath L, Elmquist G, et al. Distinct functional properties of murine perinatal and adult adipose progenitor subpopulations. Nat Metab 2022;4:1055–70.
[19] Burl RB, Ramseyer VD, Rondini EA, Pique-Regi R, Lee Y-H, Granneman JG, et al. Deconstructing adipogenesis induced by β3-Adrenergic receptor activation with single-cell expression profiling. Cell Metab 2018;28:300–309.e4.
[20] Schwalie PC, Dong H, Zachara M, Russeil J, Alpern D, Akchiche N, et al. A stromal cell population that inhibits adipogenesis in mammalian fat depots. Nature 2018;559:103–8.
[21] Klingelhutz AJ, Gourronc FA, Chaly A, Wadkins DA, Burand AJ, Markan KR, et al. Scaffold-free generation of uniform adipose spheroids for metabolism research and drug discovery. Sci Rep 2018;8:523.
[22] Massier L, Jalkanen J, Elmastas M, Zhong J, Wang T, Nankam PAN, et al. An integrated single cell and spatial transcriptomic map of human white adipose tissue. Nat Commun 2023;14:1438.
[23] Klingelhuber F, Frendo-Cumbo S, Omar-Hmeadi M, Massier L, Kakimoto P, Taylor AJ, et al. A spatiotemporal proteomic map of human adipogenesis. Nat Metab 2024;6:861–79.
[24] Langhardt J, Flehmig G, Klöting N, Lehmann S, Ebert T, Kern M, et al. Effects of weight loss on glutathione peroxidase 3 serum concentrations and adipose tissue expression in human obesity. Obes Facts 2018;11:475–90.
[25] Klöting N, Fasshauer M, Dietrich A, Kovacs P, Schön MR, Kern M, et al. Insulin-sensitive obesity. Am J Physiol Endocrinol Metab 2010;299:E506–15.
[26] Arndt L, Lindhorst A, Neugebauer J, Hoffmann A, Hobusch C, Alexaki V-I, et al. The role of IL-13 and IL-4 in adipose tissue fibrosis. Int J Mol Sci 2023;24:5672.
[27] Hepler C, Vishvanath L, Gupta RK. Sorting out adipocyte precursors and their role in physiology and disease. Genes Dev 2017;31:127–40.
[28] Long JZ, Svensson KJ, Tsai L, Zeng X, Roh HC, Kong X, et al. A smooth muscle-like origin for beige adipocytes. Cell Metab 2014;19:810–20.
[29] Dufau J, Shen JX, Couchet M, Barbosa TDC, Mejhert N, Massier L, et al. In vitro and ex vivo models of adipocytes. Am J Physiol Cell Physiol 2021;320:C822–41.
[30] Zhang X, Saarinen AM, Campbell LE, Filippis EAD, Liu J. Regulation of lipolytic response and energy balance by Melanocortin 2 receptor accessory protein (MRAP) in adipocytes. Diabetes 2018;67:222–34.
[31] Liu T, Elmquist JK, Williams KW. Mrap2: an accessory protein linked to obesity. Cell Metab 2013;18:309–11.
[32] Jackson DS, Ramachandrappa S, Clark AJ, Chan LF. Melanocortin receptor accessory proteins in adrenal disease and obesity. Front Neurosci 2015;9:213.
[33] Mracek T, Ding Q, Tzanavari T, Kos K, Pinkney J, Wilding J, et al. The adipokine zinc-α2-glycoprotein (ZAG) is downregulated with fat mass expansion in obesity. Clin Endocrinol 2010;72:334–41.
[34] Fan G, Dang X, Li Y, Chen J, Zhao R, Yang X. Zinc-α2-glycoprotein promotes browning of white adipose tissue in cold-exposed male mice. Mol Cell Endocrinol 2020;501:110669.
[35] Xiao X-H, Qi X-Y, Wang Y-D, Ran L, Yang J, Zhang H-L, et al. Zinc alpha2 glycoprotein promotes browning in adipocytes. Biochem Biophys Res Commun 2018;496:287–93.
[36] Qiu S, Wu Q, Wang H, Liu D, Chen C, Zhu Z, et al. AZGP1 in POMC neurons modulates energy homeostasis and metabolism through leptin-mediated STAT3 phosphorylation. Nat Commun 2024;15:3377.
[37] Banaszak M, Górna I, Przysławski J. Zinc and the innovative Zinc-α2-Glycoprotein adipokine play an important role in lipid metabolism: a critical review. Nutrients 2021;13:2023.
[38] Nagy CT, Koncsos G, Varga ZV, Baranyai T, Tuza S, Kassai F, et al. Selegiline reduces adiposity induced by high-fat, high-sucrose diet in male rats. Br J Pharmacol 2018;175:3713–26.
[39] Joung H-Y, Oh J-M, Song M-S, Kwon Y-B, Chun S. Selegiline modulates lipid metabolism by activating AMPK pathways of epididymal white adipose tissues in HFD-Fed obese mice. Pharmaceutics 2023;15:2539.
[40] Oort PJ, Warden CH, Baumann TK, Knotts TA, Adams SH. Characterization of Tusc5, an adipocyte gene co-expressed in peripheral neurons. Mol Cell Endocrinol 2007;276:24–35.
[41] Knotts TA, Lee HW, Kim JB, Oort PJ, McPherson R, Dent R, et al. Molecular characterization of the tumor suppressor candidate 5 gene: regulation by PPARγ and identification of TUSC5 coding variants in lean and Obese humans. PPAR Res 2009;2009:867678.
[42] Beaton N, Rudigier C, Moest H, Müller S, Mrosek N, Röder E, et al. TUSC5 regulates insulin-mediated adipose tissue glucose uptake by modulation of GLUT4 recycling. Mol Metabol 2015;4:795–810.
[43] Brady MJ, Nairn AC, Saltiel AR. The regulation of glycogen synthase by protein phosphatase 1 in 3T3-L1 adipocytes evidence for a potential role for darpp-32 in insulin action*. J Biol Chem 1997;272:29698–703.
[44] Bulaklak K, Gersbach CA. The once and future gene therapy. Nat Commun 2020;11:5820.
[45] Hoang DM, Pham PT, Bach TQ, Ngo ATL, Nguyen QT, Phan TTK, et al. Stem cell-based therapy for human diseases. Signal Transduct Targeted Ther 2022;7:272.
[46] Wood KJ, Fry J. Gene therapy: potential applications in clinical transplantation. Expet Rev Mol Med 1999;1:1–20.
[47] Zhang H, Kumar S, Barnett A, Eggo M. Ceiling culture of mature human adipocytes: use in studies of adipocyte functions. J Endocrinol 2000;164:119–28.
[48] Matsumoto T, Kano K, Kondo D, Fukuda N, Iribe Y, Tanaka N, et al. Mature adipocyte-derived dedifferentiated fat cells exhibit multilineage potential. J Cell Physiol 2008;215:210–22.
[49] Dobin A, Davis CA, Schlesinger F, Drenkow J, Zaleski C, Jha S, et al. STAR: ultrafast universal RNA-seq aligner. Bioinformatics 2013;29:15–21.
[50] Howe KL, Achuthan P, Allen J, Allen J, Alvarez-Jarreta J, Amode MR, et al. Ensembl 2021. Nucleic Acids Res 2020;49:gkaa942.
[51] Butler A, Hoffman P, Smibert P, Papalexi E, Satija R. Integrating single-cell transcriptomic data across different conditions, technologies, and species. Nat Biotechnol 2018;36:411–20.
[52] Tirosh I, Izar B, Prakadan SM, II MHW, Treacy D, Trombetta JJ, et al. Dissecting the multicellular ecosystem of metastatic melanoma by single-cell RNA-seq. Science 2016;352:189–96.
[53] Schlager S, Salomon C, Olt S, Albrecht C, Ebert A, Bergner O, et al. Inducible knock-out of BCL6 in lymphoma cells results in tumor stasis. Oncotarget 2020;11:875–90.
[54] Ritchie ME, Phipson B, Wu D, Hu Y, Law CW, Shi W, et al. Limma powers differential expression analyses for RNA-sequencing and microarray studies. Nucleic Acids Res 2015;43:e47.
[55] Law CW, Chen Y, Shi W, Smyth GK. Voom: precision weights unlock linear model analysis tools for RNA-seq read counts. Genome Biol 2014;15:R29.
[56] Picelli S, Faridani OR, Björklund ÅK, Winberg G, Sagasser S, Sandberg R. Full-length RNA-seq from single cells using Smart-seq2. Nat Protoc 2014;9:171–81.
[57] Chen S, Zhou Y, Chen Y, Gu J. Fastp: an ultra-fast all-in-one FASTQ preprocessor. Bioinformatics 2018;34:i884–90.
[58] Bray NL, Pimentel H, Melsted P, Pachter L. Near-optimal probabilistic RNA-seq quantification. Nat Biotechnol 2016;34:525–7.
[59] Love MI, Huber W, Anders S. Moderated estimation of fold change and dispersion for RNA-seq data with DESeq2. Genome Biol 2014;15:550.
[60] Wang L, Nie J, Sicotte H, Li Y, Eckel-Passow JE, Dasari S, et al. Measure transcript integrity using RNA-seq data. BMC Bioinf 2016;17:58.
[61] Wang L, Wang S, Li W. RSeQC: quality control of RNA-seq experiments. Bioinformatics 2012;28:2184–5.

